

## Imaging developing neural morphology using optical coherence tomography

Stephen A. Boppart<sup>a,\*</sup>, Brett E. Bouma<sup>b</sup>, Mark E. Brezinski<sup>c</sup>, Guillermo J. Tearney<sup>b</sup>,  
James G. Fujimoto<sup>b</sup>

<sup>a</sup> Harvard-MIT Division of Health Sciences and Technology, Department of Electrical Engineering and Computer Science, Research Laboratory of Electronics, Massachusetts Institute of Technology, Cambridge, MA 02139, USA

<sup>b</sup> Department of Electrical Engineering and Computer Science, Research Laboratory of Electronics, Massachusetts Institute of Technology, Cambridge, MA 02139, USA

<sup>c</sup> Cardiac Unit, Massachusetts General Hospital, Harvard Medical School, Boston, MA 02114, USA

Received 11 April 1996; revised 28 June 1996; accepted 29 June 1996

### Abstract

Imaging technologies offer numerous possibilities to investigate the processes involved in neural development. The optical coherence tomography (OCT) technology is analogous to ultrasound backscatter microscopy except reflections of light are detected rather than sound. The OCT technology combines high-resolution in vivo imaging in a diode-based benchtop instrument capable of micron-scale resolution in transparent and non-transparent biological specimens. In this paper, we examine the potential of using OCT for the investigation of developing neural morphology. To demonstrate the capabilities of this technique in assessing neural development, we have chosen to image early normal and abnormal neural morphology in a common developmental biology model, *Xenopus laevis*. In vivo images clearly identify gross and subtle differences in neural structure and may offer an alternative to the costly and time-consuming process of repeated histological preparation for neural developmental studies. Because imaging can be performed rapidly and repeatedly, the morphological changes of single specimens can be followed throughout development. To illustrate the future potential of this technique, a state-of-the-art Cr<sup>4+</sup>:forsterite modelocked laser is used as a broad bandwidth light source to image individual cells in a developing specimen.

**Keywords:** Imaging; Development; Embryology; Microscopy; Optics; *Xenopus laevis*

### 1. Introduction

To understand the complex processes that occur during neural development, a means of visualizing these micron-scale changes is necessary, often in semi-transparent and opaque specimens. Imaging modalities such as computed tomography (CT), magnetic resonance imaging (MRI), and ultrasound (US) are examples of well-recognized technologies that have been developed through physics and engineering, but have had a significant impact on the medical community as a means of visualizing internal in vivo biological structure. Unfortunately, the CT and MRI technologies are often slow, require ample laboratory space,

and require skilled operators to acquire quality images. Because of this, their use as benchtop instruments is limited. Additionally, resolutions from clinically based systems on the order of 100  $\mu\text{m}$  have limited the use of these technologies for microscopic investigation of specimens and have pushed investigators toward engineering high-resolution systems. MRI imaging with 12  $\mu\text{m}$  resolution has been applied to observing the early developmental changes in *Xenopus* embryos (Jacobs and Fraser, 1994a,b). However, the long image acquisition times and the complexity of the instrument will make laboratory implementation difficult. High-resolution CT imaging has been performed on fixed insect specimens (Morton et al., 1990), but does not appear suitable for any in vivo developmental investigations. Using high-frequencies (40–100 MHz), ultrasound backscatter microscopy has shown promise for imaging the in vivo development of mice and for identify-

\* Corresponding author. Tel: +1 (617) 253-8520; Fax: +1 (617) 253-9611; E-mail: boppart@mit.edu

ing developmental abnormalities in neural tube closure (Turnbull et al., 1995). Ultrasound probes require contact with the specimen for imaging.

The development of confocal microscopy (CM) (Minsky, 1988) has revolutionized the manner in which biological specimens are visualized. With high contrast and sensitivity, confocal systems have shown improved performance compared to light microscopy by rejecting out-of-plane light (spatially filtering). This modality has been well implemented in the laboratory environment. There are, however, limitations to CM. To achieve high imaging depths of penetration and maintain high resolutions, specimens must be relatively transparent. Hence, CM is limited to imaging biological structure to depths of less than a few hundred microns. To enhance contrast using laser-scanning confocal microscopy, fluorophores are used to label specific cells or sub-cellular constituents. Extended excitation of these fluorophores, however, leads to the production of toxic by-products which affect the viability of the developing specimen. Typically, most specimens must be histologically fixed before examination although, recently, there has been successful *in vivo* investigations of calcium dynamics following egg fertilization in sea urchins (Stricker et al., 1992) and *Xenopus* oocytes (Girard and Clapham, 1993).

There is a need for a versatile biological imaging tool that can be used at the level of the benchtop for high-resolution *in vivo* imaging in both transparent and non-transparent specimens. This manuscript investigates the potential of optical coherence tomography (OCT) to provide rapid and repeatable high-resolution, *in vivo* imaging for the investigation of developing neural morphology.

## 2. Materials and methods

### 2.1. Optical coherence tomography

The principles and physics of OCT have been previously described (Huang et al., 1991) but will be summarized here. This technique measures the intensity of optical backscatter at highly localized regions within a specimen. OCT is analogous to ultrasound except optical reflections, rather than acoustic reflections, are detected. The echo delay time of light returning from the specimen cannot be measured directly by electronic methods, as in ultrasound, due to the high speeds associated with the propagation of light. Therefore, an optical technique known as interferometry is used. To measure the precise depth and magnitude of each reflection, OCT incorporates a fiber-optic based Michelson interferometer. A schematic of the OCT device is shown in Fig. 1.

Optical coherence tomography has the ability to image specimens that are opaque to visible light because it utilizes wavelengths of light in the near-infrared region. Although most tissues appear opaque under visible light,

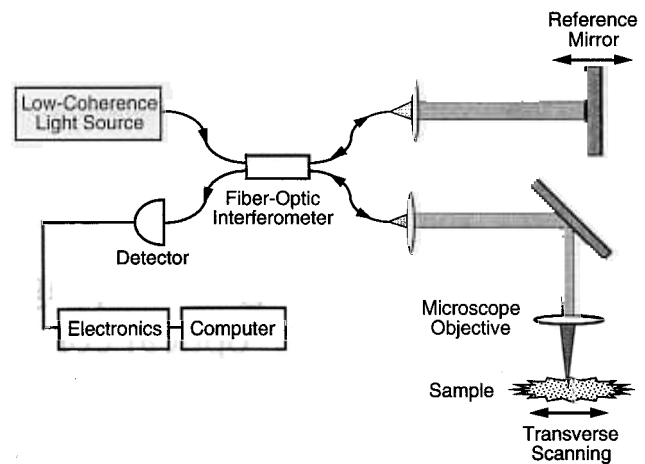


Fig. 1. Schematic diagram of the optical coherence tomography (OCT) imaging system. The OCT system uses fiber optics and a compact diode light source. The light source is coupled into a fiber splitter which functions like a Michelson interferometer. One of the fibers directs light to the tissue being imaged and the other to a moving reference mirror. By using a low coherence length light source and measuring the interference between light backscattered from the tissue and from the reference mirror, the distance and magnitude of optical scattering within the tissue can be measured with micron-scale precision. A cross-sectional image is produced by scanning the light beam across the tissue while the axial reflectance profiles at each transverse position are recorded by computer. The result is a two-dimensional representation of the optical backscatter of the tissue in cross-section, which is displayed in grey-scale.

they are relatively non-absorbing in the near infrared. Imaging depth is therefore limited by optical scattering and attenuation rather than absorption. Using a 1300 nm low-coherent super-luminescent diode as a light source, light is split equally by a fiber coupler with half sent to the reference arm and half sent to the sample arm of the interferometer. A computer-controlled scanning reference arm mirror sets the depths at which backscattering will be measured. Light sent to the sample arm is focused into the tissue. Reflections or backscatter from both arms are recombined by the fiber coupler and detected with a photodiode. Interference between the two arms only occurs when their path lengths are matched to within the coherence length of the source. Thus, the coherence length of the source determines the axial resolution. The 50 nm spectral bandwidth of this super-luminescent diode (the axial resolution is inversely proportional to the spectral bandwidth) yields a free-space axial resolution of 16  $\mu\text{m}$ . The resolution was verified by measuring the point spread function off of a mirror placed in the sample arm. The 30  $\mu\text{m}$  transverse resolution is determined by the spot size of the incident beam within the specimen. Optical focusing properties force a trade-off between a high transverse resolution and a high depth of field. The 30  $\mu\text{m}$  transverse resolution was optimally selected to provided a confocal parameter (depth of field) of 1.1 mm without significant loss in transverse resolution. High numerical aperture ob-

jectives could be used to increase transverse resolutions to those comparable with confocal and light microscopy at the expense of extremely short confocal parameters. An anti-reflection lens coated for the source wavelength to eliminate secondary backreflections was used to focus the beam into the specimen. These resolutions are consistent for all the images in this paper that were acquired using the super-luminescent diode as a light source.

The average index of refraction of the *Xenopus* specimen was determined to be 1.35 (Tearney et al., 1995). The axial resolution within the specimen is therefore the free-space resolution divided by the index of refraction or 12  $\mu\text{m}$ . This in vivo resolution was confirmed by measuring from an image the separation distance at which two converging structures could no longer be distinctly resolved. For the cornea/lid and iris/cornea anterior chamber angles of the tadpole eye, the in vivo resolution was measured to be 12–14  $\mu\text{m}$ . The signal-to-noise ratio was measured at 109 dB, with only 160  $\mu\text{W}$  incident on the specimen. The signal-to-noise ratio was determined by measuring the maximal detected power when the optical beam is reflected from a high reflecting mirror divided by the variance of the background noise level of the instrument. Images were generated by displaying the logarithm of the backscattered intensity vs. position in gray-scale. Imaging depths up to 3 mm were possible in scattering tissue with acquisition times for each image between 15 and 40 s.

The imaging capabilities of OCT have been well documented for the transparent tissue found in the eye (Hee et al., 1995; Puliafito et al., 1995; Drexler et al., 1995). Recently, OCT has been effective at imaging pathologic structure in highly scattering tissue due to its ability to reject multiply scattered photons (Schmitt et al., 1994; Fujimoto et al., 1995; Pan et al., 1995). With the ability to optically biopsy tissue, OCT has provided clinically relevant images of atherosclerotic plaques in in vitro human coronary arteries (Brezinski et al., 1996).

Because OCT has the ability to acquire optical histology from tissue or specimens without the need to excise tissue or to sacrifice, images can be acquired over time to reveal a time-evolution of the dynamic structural changes that occur. Cross-sectional scans acquired temporally can be sequenced to produce a time-lapse movie to characterize the dynamics of the tissue during cellular differentiation. Because of the computer-controlled micron-precision stages, scans acquired spatially at regular intervals across specimens maintain perfect image registration and can be reconstructed to produce a three-dimensional image of the biological structure. From this 3-D data set, serial sectioning can be performed by computer at arbitrary planes to highlight particular anatomical structures. These techniques can be directly applied to improve the imaging capabilities of developing neural morphology by providing a three- and four-dimensional ( $x$ ,  $y$ ,  $z$ , time) picture of the dynamic processes during development.

## 2.2. Specimen preparation

To characterize the ability of OCT to image developing neural morphology, a common developmental biology model, *Xenopus laevis*, was chosen for our studies. *Xenopus* embryos were obtained 1 h after fertilization and maintained in a solution of  $0.10 \times \text{MBS}$  (modified Barth's saline) at room temperature with a 12 h light-dark cycle. Embryos were fed a prepared diet of *Xenopus* nutrient (Connecticut Valley Biological) once daily. Three specimens were used to acquire the images shown in this paper and all imaging was performed at room temperature. At stage 51 (day 17), the first specimen was immersed in 0.05% Tricaine for 5 min until the specimen no longer responded to touch. In vivo imaging was performed by orienting the specimen in a clay-lined dish so the light beam from the OCT sample arm was incident on the dorsal side. The position of the invisible infrared (1300 nm) OCT beam on the specimen was monitored with a visible (632 nm) guiding beam coincident with the imaging beam. Immediately following image acquisition, the specimen was returned to the 0.05% Tricaine for 1 h until no cardiac activity was observed. The specimen was then transferred to a 10% buffered solution of formaldehyde for later standard histological preparation. Histological sections were obtained every 20  $\mu\text{m}$ , perpendicular to the antero-posterior axis, and stained with hematoxylin and eosin (H&E). Numerous OCT images had been obtained every 25–50  $\mu\text{m}$ . From these, images were selected based on correspondence with histology.

The second (stage 48) and third (stage 47) specimens were anaesthetized with 0.05% Tricaine. Following immersion for 5 min, each specimen no longer responded to touch and was positioned in the OCT sample arm for in vivo imaging. Immediately following imaging, the specimen was returned to the housing. Within 30 min, the specimen appeared to recover fully and to proceed with normal activity.

The animals used in this study were cared for and maintained under the established protocols of the Committee on Animal Care, Massachusetts Institute of Technology.

## 3. Results

To demonstrate the potential of OCT to image in vivo developing neural morphology in a specimen which is not transparent, but scattering, a sagittal section through a *Xenopus* brain is shown in Fig. 2. This image ( $2 \times 6 \text{ mm}$ ,  $250 \times 500$  pixels) was acquired in 40 s and represents a 30  $\mu\text{m}$  thick (spot size) optical slice of the specimen. This image was created by aligning the OCT imaging beam on the dorsal side of the specimen for a scan parallel to the anteroposterior axis. At one transverse position, a vertical column (axial scan) of 250 pixels of data was collected

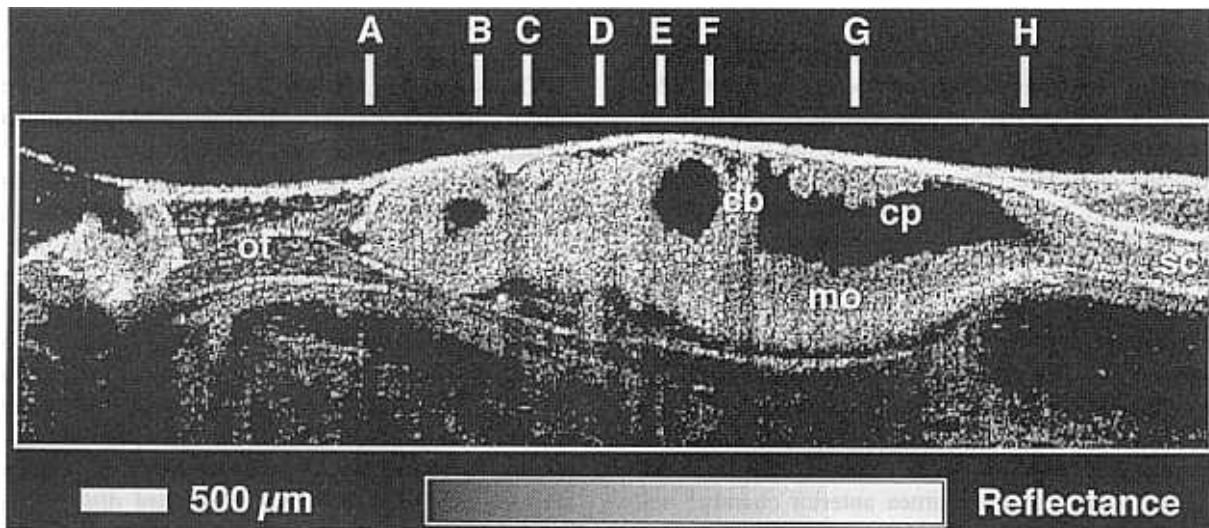


Fig. 2. In vivo sagittal OCT image of *Xenopus* brain, nasal placode, and surrounding structure. With  $12\ \mu\text{m}$  resolution, internal neural morphology in this non-transparent, scattering tissue is clearly identified. Grey-scale bar indicates intensity of optical backscatter. Neural tissue appears more highly backscattering (grey to white) compared to the low backscattering cerebral spinal fluid (black). Vertical labeled lines correspond to locations of cross-sectional images shown in Fig. 3. cb, cerebellum; cp, choroid plexus; mo, medulla oblongata; ot, olfactory tract; sc, spinal cord.

corresponding to the intensity of optical backscattering within the specimen. The specimen was then translated by a computer-controlled stage in a transverse direction and

adjacent axial scans were assembled to produce this two-dimensional image. The logarithm of the data was assigned a grey-scale table and displayed. The grey-scale bar, there-

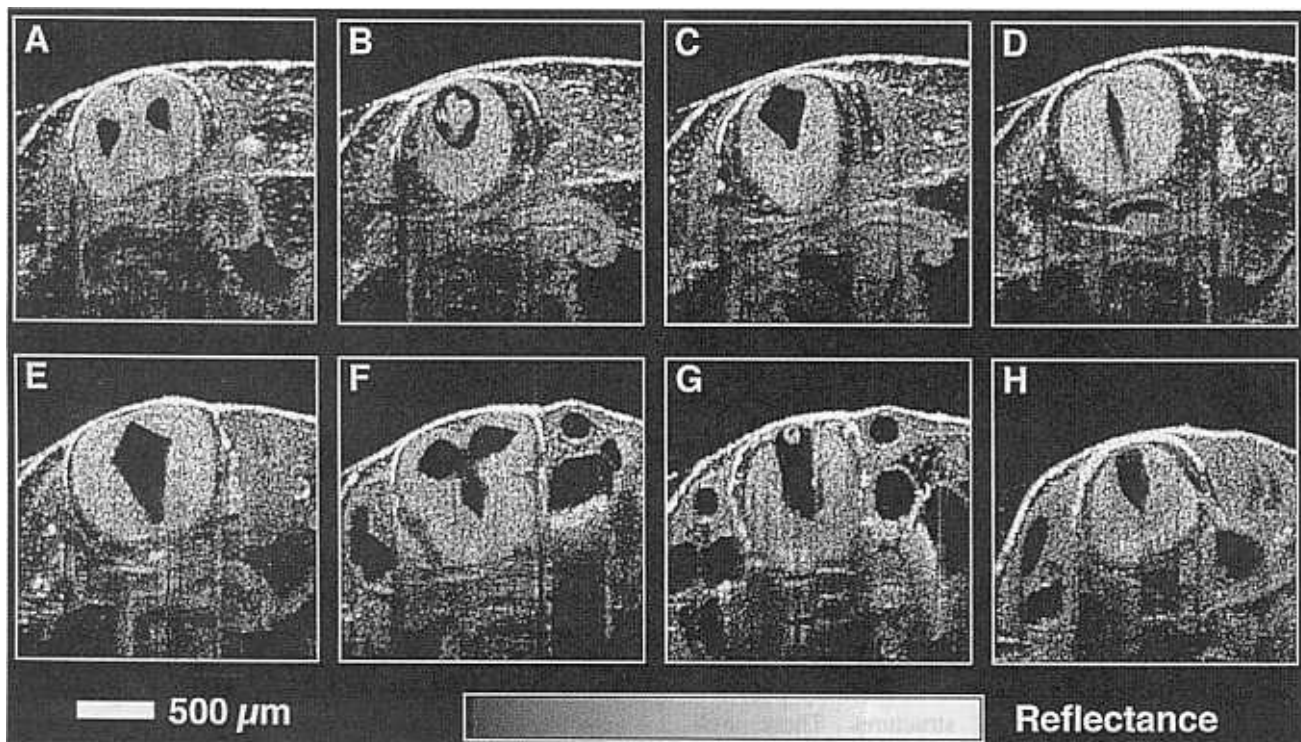


Fig. 3. Corresponding cross-sections of the *Xenopus* brain morphology shown in Fig. 2. Images were acquired perpendicular to the anteroposterior axis and illustrate normal developing morphology. Panel A shows the paired cerebral hemispheres of the telencephalon and the two lateral ventricles. Panel D illustrates the narrowing of the aqueduct of Sylvius connecting the diocoel with the rhombocoel. The posterior choroid plexus, which is on the order of  $50\text{--}100\ \mu\text{m}$ , is clearly resolved in the fourth ventricle in panel G.

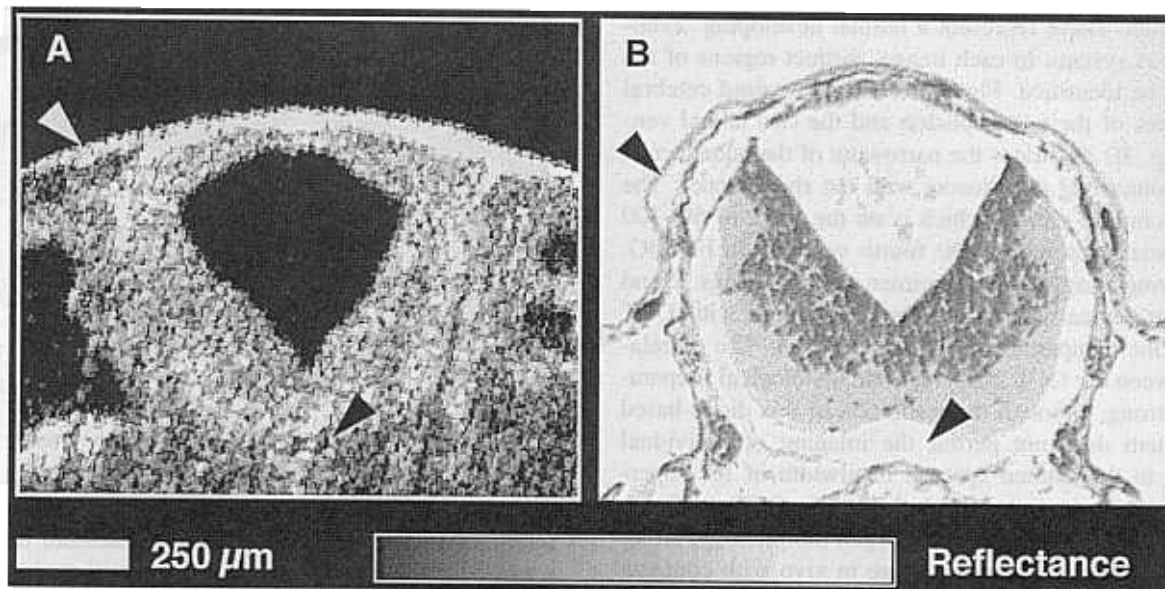


Fig. 4. Comparison of OCT cross-sectional imaging of *Xenopus* rhombencephalon morphology with corresponding histology. Histological section was stained with H&E. Arrows indicates preparation artifacts that can be identified after comparison with OCT image. OCT imaging can be performed rapidly and repeatedly and maintains the in vivo orientation of morphology.

fore, indicates the intensity of optical backscatter spanning a range of approx.  $-60$  to  $-110$  dB with white representing the highest backscattered signal. This image shows high-resolution detail of internal brain morphology. Structures corresponding to the cerebellum, choroid plexus, and medulla oblongata are identified as well as a longitudinal section of the nasal tube and olfactory nerve as it enters the nasal placode. The dark internal regions correspond to

the low-backscattering cerebral spinal fluid within the lateral, third, and fourth ventricles. Posteriorly, a longitudinal section of the spinal cord is observed.

The vertical labeled lines in Fig. 2 correspond to planes where cross-sectional OCT images were acquired from this same specimen. These images ( $1.5 \times 1.5$  mm,  $200 \times 200$  pixels), each obtained in 15 s, are shown in Fig. 3 and were acquired perpendicular to the anteroposterior axis of

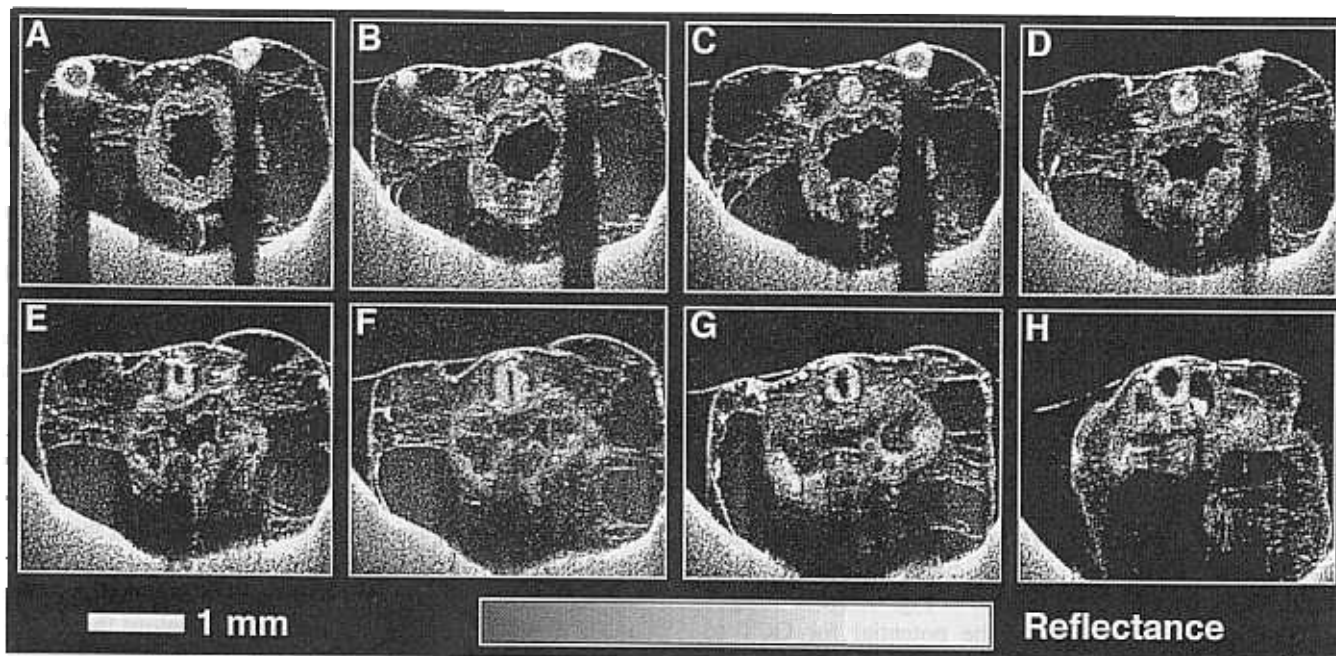


Fig. 5. Representative series of cross-sectional images of abnormal neural development. Images were acquired every  $200 \mu\text{m}$  along the anteroposterior axis of the specimen. The neural tube, eyes, and abnormal body organization can be identified. The highly backscattering ocular structures produces a shadowing effect on the tissue below. This effect is seen as dark vertical bands in images A–C. Sequence illustrates the potential of reconstructing a three-dimensional representation of the specimen as well as the opportunity to investigate other developing organ systems. Specimen is resting in a contoured, clay-lined dish.

the specimen. These represent a normal developing *Xenopus* nervous system. In each image, distinct regions of the brain can be identified. Fig. 3A shows the paired cerebral hemispheres of the telencephalon and the two lateral ventricles. Fig. 3D illustrates the narrowing of the aqueduct of Sylvius connecting the diocoel with the rhombocoel. The posterior choroid plexus, which is on the order of 50–100  $\mu\text{m}$ , is clearly resolved in the fourth ventricle in Fig. 3G.

Following imaging, the specimen shown in Figs. 2 and 3 was histologically prepared for comparison with OCT images. One comparison is shown in Fig. 4. The correlations between the OCT image and the histological preparation are strong, although the resolution of this diode-based OCT system does not permit the imaging of individual cells due to the limited spectral bandwidth of the super-luminescent diode light source. Instead, OCT performs well at imaging larger tissue and organ morphology; structure that is often too large to image *in vivo* with confocal microscopy. Note, however, the presence of preparation artifacts indicated by the arrows in Fig. 4B. The top arrow indicates the displaced outer membrane of the embryo. The bottom arrow points to neural tissue separation from the surrounding structure. These artifacts are most likely the result of dehydration of the tissue during processing or dislocations from sectioning and are relatively common. The OCT image in Fig. 4A closely preserves the *in vivo* orientation and can be used to identify questionable artifacts found in the histology. The arrows in the OCT image point to the *in vivo* location where histological processing artifacts occurred. OCT images have their own specific artifacts based on the optical properties of the tissue and include the attenuation of signal with increasing depth and shadowing of deeper morphology from backscattering structures.

The ability of OCT to sample abnormal developing neural structure is shown in Fig. 5. Cross-sections of an abnormal specimen were acquired every 200  $\mu\text{m}$  along the anteroposterior axis as the specimen rested in a clay-lined dish. Representative images are shown. The abnormalities are believed to be spontaneous and not the result of any mutagenic agents. Representative images ( $3 \times 3.5$  mm,  $300 \times 350$  pixels, 35 s acquisition) show a poorly developing nervous system as well as a greatly distorted body pattern. The developing optic cups are oriented dorsally rather than more lateral. Images in Fig. 5A and B show portions of the left optic nerve and ocular muscles. The neural tube can be readily identified in each image in this sequence. To highlight particular neural abnormalities, imaging can be limited to just the brain or neural tube as was done for the normal specimen in Fig. 4. These images are also intended to illustrate the potential for OCT to image many other systems within the developing specimen as imaging is possible through the entire specimen and into the clay. The highly backscattering ocular tissue in Fig. 5C produces a shadowing effect on the underlying tissue below. As incident light travels through the specimen,

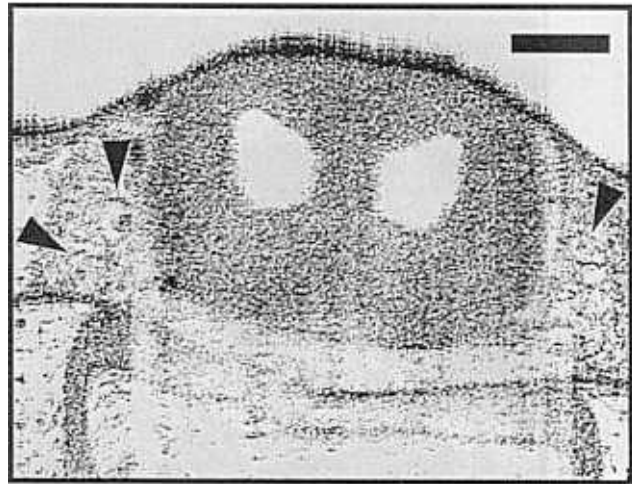


Fig. 6. High-resolution OCT image acquired using a 1280 nm wavelength, modelocked  $\text{Cr}^{4+}$ :forsterite laser. The increased optical bandwidth of the laser source results in a 5  $\mu\text{m}$  axial resolution. At this resolution, individual cells can be resolved (arrows) along with cell membranes and nuclei. Increased artifacts are observed along the air/specimen interface due to the large discontinuity in index of refraction and the non-Gaussian optical spectrum from the laser. These artifacts are not present within the specimen where changes in index are less significant. The use of this laser system, however, requires considerable laboratory space. Bar = 250  $\mu\text{m}$ .

photons are either scattered or absorbed. At regions deep within the specimen or in areas below scattering structures, less light is available to be backscattered and, hence, the signal-to-noise ratio is lowered and the region appears faint. The shadowing that is observed below the ocular tissue is an extreme example of this effect. It is difficult to predict when this effect will be significant. For example, the neural tube and brain in these images are scattering structures yet little shadowing is observed. In fact, high contrast is still present in the tissue structures below.

The previous images were all obtained using a compact super-luminescent diode source which provided 12  $\mu\text{m}$  axial resolution. To demonstrate the future potential of OCT for imaging at cellular resolutions, a state-of-the-art, modelocked  $\text{Cr}^{4+}$ :forsterite laser was used as a 1280 nm wavelength light source. An *in vivo* image with 5  $\mu\text{m}$  axial and 13  $\mu\text{m}$  transverse resolution is shown in Fig. 6. On either side of the cerebral hemispheres, several individual mesenchymal cells can be identified (arrows). Cell membranes and nuclei can begin to be resolved at this resolution. The higher 2 mW power incident on the specimen and the irregularities in the broadened spectrum from the forsterite laser result in additional image artifacts such as the loss of sharp boundaries between regions that have a large discontinuity in index of refraction, like the air/specimen interface. These artifacts, however, do not occur within the specimen where variations in index of refraction are reduced. The use of this modelocked laser requires an additional Nd:YAG pump laser, an optical

table, and substantial laboratory space. Thus, in this configuration, the OCT instrument can no longer be considered a benchtop device.

#### 4. Discussion

Optical coherence tomography fills a niche between confocal microscopy and imaging modalities such as US, MRI, and CT. Specimens or morphology too large for light and confocal microscopy can still be imaged with high resolution using OCT. The cost, complexity, or size of other imaging technologies is sometimes prohibitive for routine, benchtop imaging. We have shown that a diode-based benchtop OCT instrument provides 12  $\mu\text{m}$  resolution with 3 mm of imaging penetration in *X. laevis* tadpoles, a common developmental biology model. The imaging capabilities of OCT will greatly extend the ability to investigate neural development. OCT can complement the en face view of light microscopy by allowing imaging to be performed from the transverse, cross-sectional perspective. OCT will also enable the visualization of neural development in more scattering, optically opaque specimens, and in some adult animal models.

The OCT technology is based on fiber optics which are used in the field of optical communication. Hence, the system is reliable and low-cost. Apart from a personal computer for image acquisition, processing, and display, the OCT instrument is contained in a box no larger than a modern oscilloscope. This compact and portable device can be readily integrated with current clinical and laboratory optical instruments including ophthalmic instrumentation (Hee et al., 1995), catheters and endoscopes, and modified light microscopes.

Sagittal and cross-sectional neural morphology in developing *Xenopus* embryos has been imaged with high-resolution and identified using optical coherence tomography. The ability of OCT to image with high penetration depths in non-transparent, scattering specimens beyond the ranges of confocal and light microscopy enhances the identification of in vivo and in vitro morphological structure. The ability to recognize both normal and abnormal developing neural morphology has the potential for identifying mutations and neurological defects resulting from genetic disease, environmental toxins, or predetermined genetic manipulations.

Acquired OCT images compare favorably to corresponding histology. The images, however, should not be interpreted in the same manner as histology. Contrast in histological preparations relies on the differential staining properties of the tissue and the transmission of light through the section. OCT image contrast is dependent on the differences in optical backscatter between tissue microstructure. From the results of our investigation, OCT images accurately represent the neural morphology in the in vivo specimen.

High-quality histology is often difficult to obtain, costly, and time consuming for these small, fragile specimens. It is also impractical to histologically prepare the large numbers of specimens typically needed for genetic and developmental studies. OCT offers a significant alternative for rapidly accessing morphological changes. Used as a research tool for near real-time optical histology, OCT may reduce the need to sacrifice specimens. The use of OCT may also reduce the uncertainty associated with artifacts often attributed to histological preparation by identifying the in vivo orientation of the specimen and the biological structure prior to processing.

OCT images of the developing *Xenopus* central nervous system can be used to provide useful qualitative information of the variations during development. Images can be used to obtain quantitative information as well since images were assembled with precise computer-controlled alignment and scanning. The acquisition times used in this study are inadequate for real-time imaging, but imaging time may be reduced significantly. Instrument improvements include increasing laser source power, scanning speed, and the redesign of electronics. These improvements are straightforward and should lead to substantial reductions in imaging time. The use of piezoelectric cylinders to stretch coiled optical fiber has offered a high-speed, non-mechanical alternative for rapid axial scanning and permitted acquisition rates of 4 images per s (Tearney et al., 1996). Real-time acquisition of data will reduce the likelihood of specimen motion artifacts with the potential for images to be obtained without the need to anaesthetize specimens. Improved data acquisition rates will also enable 3-D data sets to be rapidly acquired over time, permitting analysis of the dynamic morphological changes that occur during development.

Significant technological advances will only serve to improve the ability of OCT to image and identify subtle structural features. New laser sources at other wavelengths in the near-infrared will potentially reveal new information since tissue scattering and absorbance properties in specimens depend highly on wavelength. Shorter coherence-length laser sources have already permitted resolutions on the order of 2–5  $\mu\text{m}$  (Clivaz et al., 1994; Bouma et al., 1995). These higher resolutions permit the imaging of individual cells. Although these cellular resolutions provide more morphological detail, the use of modelocked lasers requires a considerable amount of technical skill in order to align, operate, and maintain these systems. Typically, a modelocked laser system requires significant laboratory space to accommodate an optical table and large, water-cooled, argon or Nd:YAG pump lasers. Advances in diode-pumped fiber laser sources may provide the larger optical bandwidths for cellular resolutions in a compact instrument no larger than the current benchtop diode-based OCT system.

In theory, there is the potential for developing an OCT molecular probe that would allow cellular movements to

be followed on a macro-cellular level. It may be possible to utilize melanin granules or air-filled albumin microspheres to vary the absorption or reflectance properties in labeled cells or tissues. Cell fate and lineage analysis could be performed millimeters deep within living, developing embryos that appear opaque in visible light. The fiber-based design of OCT allows for very small sample arm beam delivery systems such as a fiber-optic imaging catheter. Such a catheter can be used in utero to examine neural development in live-bearing species.

In conclusion, the OCT technology is capable of imaging the developing nervous system in *Xenopus* and offers many new possibilities for understanding developmental processes. We have shown that optical coherence tomography provides high-resolution structural information on the *Xenopus* brain while demonstrating a feasibility to gain further insight into the morphological expression of the genetic program during development. High-resolution optical histology permits the in vivo identification of abnormal morphological variations during embryogenesis. Optical coherence tomography represents a multifunctional, investigative, benchtop tool that could complement many of the existing imaging technologies and instruments available today. This technique has the potential to contribute significantly to the investigation of the developing nervous system.

### Acknowledgements

The authors would like to thank Dr. Hazel Sive and her laboratory personnel of the Massachusetts Institute of Technology for providing us with *X. laevis* specimens and advice on the care and handling of embryos. The contributions of E.A. Swanson of MIT Lincoln Laboratory and J.F. Southern of Siani Samariton Medical Center, Milwaukee, WI are also greatly appreciated. This work was supported by NIH grant NIH-9-RO1-EY11289-10, the Office of Naval Research Medical Free Electron Laser Program contract N00014-94-1-0717, and the Air Force Palace Knight Program.

### References

Bouma, B.E., Tearney, G.J., Boppart, S.A., Hee, M.R., Brezinski, M.B. and Fujimoto, J.G. (1995) High resolution optical coherence tomographic imaging using a modelocked Ti:Al<sub>2</sub>O<sub>3</sub> laser source, *Opt. Lett.*, 20: 1486–1488.

- Brezinski, M.E., Tearney, G.J., Bouma, B.E., Izatt, J.A., Hee, M.R., Swanson, E.A., Southern, J.F. and Fujimoto, J.G. (1996) Optical coherence tomography for optical biopsy: Properties and demonstration of vascular pathology, *Circulation*, 93: 1206–1213.
- Clivaz, X., Marquis-Weible, F. and Salathe, R.-P. (1994) In: *European Biomedical Optics Conf, SPIE Proceedings*, 2083: 19.
- Drexler, W., Hitzenberger, C.K., Sattmann, H. and Fercher, A.F. (1995) Measurement of the thickness of fundus layers by partial coherence tomography, *Opt. Eng.*, 34: 701–710.
- Fujimoto, J.G., Brezinski, M.E., Tearney, G.J., Boppart, S.A., Bouma, B.E., Hee, M.R., Southern, J.F. and Swanson, E.A. (1995) Biomedical imaging and optical biopsy using optical coherence tomography, *Nat. Med.*, 1: 970–972.
- Girard, S. and Clapham, D. (1993) Acceleration of intracellular calcium waves in *Xenopus* oocytes by calcium influx, *Science*, 260: 229–232.
- Hee, M.R., Izatt, J.A., Swanson, E.A., Huang, D., Schuman, J.S., Lin, C.P., Puliafito, C.A. and Fujimoto, J.G. (1995) Optical coherence tomography of the human retina, *Arch. Ophthalmol.*, 113: 325–332.
- Huang, D., Swanson, E.A., Lin, C.P., Schuman, J.S., Stinson, W.G., Chang, W., Hee, M.R., Flotte, T., Gregory, K., Puliafito, C.A. and Fujimoto, J.G. (1991) Optical coherence tomography, *Science*, 254: 1178–1181.
- Jacobs, R.E. and Fraser, S.E. (1994a) Magnetic resonance microscopy of embryonic cell lineages and movements, *Science*, 263: 681–684.
- Jacobs, R.E. and Fraser, S.E. (1994b) Imaging neuronal development with magnetic resonance imaging (NMR) microscopy, *J. Neurosci. Methods*, 54: 189–196.
- Minsky, M. (1988) Memoir on inventing the confocal scanning microscope, *Scanning*, 10: 128–138.
- Morton, E.J., Webb, S., Bateman, J.E., Clarke, L.J. and Shelton, C.G. (1990) Three-dimensional x-ray microtomography for medical and biological applications, *Phys. Med. Biol.*, 35: 805–820.
- Pan, Y., Birngruber, R., Rosperich, J. and Engelhardt, R. (1995) Low-coherence optical tomography in turbid tissue: theoretical analysis, *Appl. Opt.*, 34: 6564–6574.
- Puliafito, C.A., Hee, M.R., Lin, C.P., Reichel, E., Schuman, J.S., Duker, J.S., Izatt, J.A., Swanson, E.A. and Fujimoto, J.G. (1995) Imaging of macular disease with optical coherence tomography (OCT), *Ophthalmology*, 120: 217–229.
- Schmitt, J.M., Knuttel, A., Yablowsky, M. and Eckhaus, M.A. (1994) Optical-coherence tomography of a dense tissue: statistics of attenuation and backscattering, *Phys. Med. Biol.*, 39: 1705–1720.
- Stricker, S.A., Centonze, V.E., Paddock, S.W. and Schatten, G. (1992) Confocal microscopy of fertilisation-induced calcium dynamics in sea urchin eggs, *Dev. Biol.*, 149: 370–380.
- Tearney, G.J., Brezinski, M.E., Southern, J.F., Bouma, B.E., Hee, M.R. and Fujimoto, J.G. (1995) Determination of the refractive index of highly scattering human tissue by optical coherence tomography, *Opt. Lett.*, 20: 2258–2260.
- Tearney, G.J., Bouma, B.E., Boppart, S.A., Golubovic, B.G., Swanson, E.A. and Fujimoto, J.G. (1996) Rapid acquisition of in vivo biological images by use of optical coherence tomography, *Opt. Lett.*, 21: 1408–1410.
- Turnbull, D.H., Bloomfield, T.S., Baldwin, H.S., Foster, F.S. and Joyner, A.L. (1995) Ultrasound backscatter microscope analysis of early mouse embryonic brain development, *Proc. Natl. Acad. Sci. USA*, 92: 2239–2243.